Science of the Total Environment 651 (2019) 2975–2984

Contents lists available at ScienceDirect

Science of the Total Environment

journal homepage: www.elsevier.com/locate/scitotenv

Molecular structure-reactivity correlations of humic acid and humin fractions from a typical black soil for hexavalent chromium reduction

Jia Zhang, Huilin Yin, Hui Wang, Lin Xu, Barnie Samuel, Jingjie Chang, Fei Liu *, Honghan Chen

Beijing Key Laboratory of Water Resources & Environmental Engineering, China University of Geosciences, Beijing 100083, China

HIGHLIGHTS

- HMr is structurally different from other humus fractions with a high content of cellulose.
- Cr(VI) removal rate decreased with progressively humus fractionation, namely HA > HMi > HMc > HMr.
- Cr(VI) reduction rates are determined by phenol content of humus instead of carboxyl.
- Cr(VI) reduction rates are also positively correlated with polarity, except for HMr.

GRAPHICAL ABSTRACT

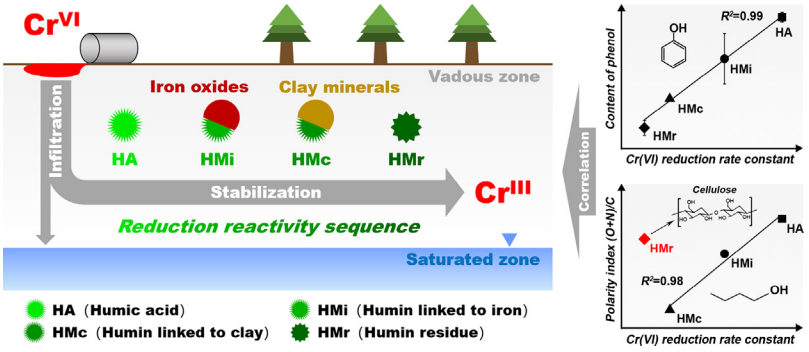

ARTICLE INFO

Article history:
Received 9 August 2018
Received in revised form 9 October 2018
Accepted 11 October 2018
Available online 12 October 2018

Editor: Jay Gan

Keywords:
Humic acid
Humin
Hexavalent chromium
Two-dimensional correlation spectroscopy
Correlation analysis

ABSTRACT

Different soil humus fractions are structurally distinct from each other molecularly, however, the relationship between their microscopic molecular structures and the macroscopic reduction of Cr(VI) is still unknown, especially for the humin fraction. In this study, different humus fractions (HA, humic acid; HMi, humin linked to iron oxides; HMc, humin linked to clay; and HMr, humin residue) were sequentially extracted from a typical black soil and well characterized. It was found that HA, HMi and HMc were the same type of humus with similar molecular structures, while HMr was structurally different from the other fractions with a high cellulose content. The removal rate of Cr(VI) in solution decreased with progressive humus fractionation, namely, HA > HMi > HMc > HMr. Based on the two-dimensional correlation spectroscopic analysis (2DCOS) of the FTIR data, the changing functional groups of all humus fractions during reacting with Cr(VI) followed a similar order: carboxyl > phenol > hydroxyl > methyl > methylene. According to the correlation analysis, Cr(VI) reduction rates by different humus fractions were mainly determined by the content of phenol ($R^2 = 0.99$) instead of carboxyl ($R^2 = 0.28$). Except for HMr, the Cr(VI) reduction rates of different humus fractions were also positively correlated with surface and bulk polarity ($R^2 = 0.98$ and 0.99) but not with aromaticity or aliphaticity ($R^2 = 0.21$).

1. Introduction

Soil organic matter (SOM) is considered as the most important factor controlling the migration and transformation of heavy metals in soils and sediments (Dai et al., 2004; Zeng et al., 2011; Zhou et al., 2018). The fractions of humus, the major component of SOM, differ greatly in their chemical composition, structures and affinity to contaminants resulting from their strong heterogeneity (Guo et al., 2013). According to the solubility in acidic and alkaline solutions, humus can be operationally classified into humic acid (HA), fulvic acid (FA) and humin (HM) (Van Zomeren and Comans, 2007). Much work thus far has

* Corresponding author.
E-mail address: feiliu@cugb.edu.cn (F. Liu).

https://doi.org/10.1016/j.scitotenv.2018.10.165
0048-9697/

focused on the interaction mechanisms between HA/FA and heavy metals (Hori et al., 2015; Janos et al., 2009; Wittbrodt and Palmer, 1995; Wittbrodt and Palmer, 1996; Wittbrodt and Palmer, 1997; Yan et al., 2016); however, relatively little information is available about the environmental significance of HM for heavy metals (Tavares Rosa et al., 2018; Wang et al., 2016; Zhang et al., 2013), which generally represents >50% of organic carbon in soils and sediments (Xing et al., 2005).

HM is operationally defined as the humus that neither dissolves in acidic nor alkaline solutions, and the degree of HM-related research is relatively low compared with HA and FA, which results from its intractable nature. The insoluble HM can be classified into two types in essence. One is the HM with apolar molecular structural characteristics resulting in its macroscopic insolubility. The other is the HM that originally can be dissolved in alkaline solutions but becomes insoluble due to it tightly binding to minerals (Fabbri et al., 1996), which is considered to be similar in properties to HA (Rice, 2001). As seen, HM itself is heterogeneous as well, and some insoluble HM isolation procedures utilizing organic solvents are available to fractionate HM into different fractions (Hayes et al., 2017; Song et al., 2011; Song et al., 2005). Dimethylsulfoxide (DMSO) and methylisobutyl ketone (MIBK) are the most common organic solvents for HM separation from the soil residue after alkaline extraction of HA and FA (Tsutsuki and Kuwatsuka, 2012; Rice and Maccarthy, 1989). Notably, Pallo (1993) reported a method of HM isolation to separate the alkaline-soluble HM bound to iron and clay minerals from the insoluble HM, by sequentially removing the iron and clay minerals with sulphuric acid and hydrofluoric acid. Accordingly, Dou et al. (2006) further classified HM into humin linked to iron oxides (HMi), humin linked to clay (HMc) and humin residue (HMr). Compared with the DMSO and MIBK method, the Pallo method gives consideration to the interaction between HM and the major inorganic minerals in soils, namely, organo-mineral complexes, which are widely distributed in soils and sediments (Bonin and Simpson, 2007). It has been demonstrated that the association of humus with minerals largely depends on their molecular weights, functional groups and aliphatic structures (Kang and Xing, 2008; Specht et al., 2000; Wang and Xing, 2005), which in turn determines that the humus fractions associated with different minerals are structurally distinct from one another in the soil environment (Li et al., 2015). Consequently, it can be inferred that the differences in properties among HA and different HM fractions would induce a dissimilar retention effect for heavy metals, especially for elements involving much more complex redox processes, such as hexavalent chromium Cr(VI), which is still unknown.

Cr(VI) is widely utilized in industries, such as electroplating, leather tanning and dyeing (Dhal et al., 2013), and quite a few instances have been reported involving the release of Cr(VI) into the subsurface environment, which has led Cr(VI) to become one of the most frequent heavy metal contaminants in soils and groundwater (Hsu et al., 2010). In the environment, Cr(VI) mainly exists in anions, such as $Cr_2O_7^{2-}$, $HCrO_4^-$ and CrO_4^{2-}, and it is quite different from Cr(III), which mainly exists in cations, such as Cr^{3+}, $Cr(OH)^{2+}$ and $Cr(OH)_2^+$ (Wittbrodt and Palmer, 1995). Humus has a great retention effect on the migration of Cr(VI) in soils and sediments (Xiao et al., 2012), and it can reduce carcinogenic and mobile Cr(VI) into less toxic and much more stable Cr(III) to mitigate its environmental risk (Jardine et al., 1999).

The organic functional groups are considered to play crucial roles in the Cr(VI) reduction by humus (Chen et al., 2011; Huang et al., 2012). It has been reported that carboxyl, phenol and hydroxyl groups might act as the main electron donors for Cr(VI) reduction by HA (Hsu et al., 2009; Lin et al., 2009; Zhao et al., 2016). Furthermore, our previous studies have demonstrated that the carboxyl of HA more preferentially tends to participate in Cr complexation instead of being oxidized by Cr(VI), while the phenol, polysaccharide and methyl of HA mainly act as the electron donors for Cr(VI) reduction (Zhang et al., 2017; Zhang et al., 2018a). However, it is still unknown whether any differences exist among HA and different HM fractions in the Cr(VI) reduction mechanism by various functional groups.

Additionally, it has been reported that the polarity and aliphaticity of HM have significant impacts on its sorption of apolar (benzo[α]phrene, phenanthrene and lindane) and polar (atrazine) organic pollutants by altering the interaction of the electrostatic force, H-bonding and van der Waals force (hydrophobic interaction) (Wang et al., 2011; Wen et al., 2007; Yang et al., 2011; Zhang et al., 2009). However, it is still unclear whether the polarity and aliphaticity have any effects on the Cr(VI) reduction by HA and different HM fractions.

The purposes of this study were to (i) compare the adsorption and reduction of Cr(VI) by HA and different HM fractions and unveil the underlying mechanisms, and (ii) probe the roles of functional groups, polarity and aliphaticity of HA and different HM fractions for Cr(VI) reduction. To achieve our aims, HA and different HM fractions, including HA, HMi, HMc and HMr, were extracted from a single soil sample to eliminate the influences of different minerals, precursors of SOM and other factors on the interaction. Additionally, in order to get a significant change in the humus spectra, a relatively high Cr/C ratio was set, and to make the reaction time scale acceptable, the reaction pH was set to 1 to accelerate the reaction rate. It should be pointed out that this pH condition is equally common in related contaminated sites, such as electroplating industries (Dermentzis et al., 2011; Hsu et al., 2007; Liu et al., 2011).

2. Materials and methods

2.1. Humus fractions extraction and characterization

The black soil sample used for humus extraction was collected from an undisturbed area at Dunhua, Jilin Province, China (43°18′36″N, 128°23′26″E), which is located at one of the three major black soil regions worldwide (the other two are the great plains of Ukraine and the Mississippi River basin of America). This black soil sample can be classified as Mollisol soil according to the soil classification system of the United States Department of Agriculture (USDA), and it is the typical black soil in the region of Northeast China. The condition of the landform, climate and vegetation were described in detail in our previous paper (Zhang et al., 2018b). The surface soil within a depth of 30 cm was sampled after the topsoil containing substantial plant roots had been removed. The soil sample was air-dried and ground, and then was passed through a 100-mesh sieve. The pre-treated soil sample was stored in a sealed brown glass bottle. The chemical characteristics of the soil are listed in Table S1.

Based on the Pallo method, with minor modifications according to the method recommended by the International Humic Substances Society (IHSS), different humus fractions were sequentially extracted, including HA, HMi, HMc and HMr. The detailed extraction procedures of different humus fractions can be found in the Supplementary Material.

The pH_{pzc} of the humus particles were determined by a zeta potential analyzer (Malvern Zetasizer Nano Z). The particle size distribution of the humus particles were determined by a particle size analyzer (Malvern Mastersizer 3000). The microscopic image of the humus particles were obtained from a scanning electron microscope (SEM, JSM 7800F). The determination methods and corresponding applied parameters for C, H, O, and N elemental contents, solid-state ^{13}C CP/MAS NMR (solid-state cross-polarization magic angle spinning ^{13}C nuclear magnetic resonance spectra), XPS (X-ray photoelectron spectroscopy spectra) and FTIR (Fourier transform infrared spectra) of all humus samples can be found in our previously published paper (Zhang et al., 2018b).

2.2. Kinetic experiment

To determine the concentration variation of Cr(VI) with time by reacting with humus, 10 ± 0.2 mg of each humus sample (HA, HMi, HMc and HMr) was mixed with 20 mL of a 2 mM Cr(VI) ($K_2Cr_2O_7$) solution in a brown bottle. The background electrolyte consisted of 0.01 M

NaCl, and the initial solution pH was adjusted to 1.0 by 2.5 M HCl. The bottles were shaken in a shaker incubator at 200 rpm at 25 °C. All experiments were run in triplicate, and a control experiment was conducted with Cr(VI) alone to clarify the Cr(VI) attenuation potential without humus. A batch of bottles was sampled at given time intervals followed by a centrifugation at 3000 rpm, and then the suspensions were filtrated with a 0.45 μm membrane. The Cr(VI) concentration in the filtrate was determined using a UV/vis spectrophotometer (SHIMADZU UV-1800) (Hsu et al., 2010). One of the three filtrated humus samples was freeze-dried for FTIR and XPS characterization. The other two samples were completely collected and dissolved with 20 mL of 0.1 M NaOH in a raw bottle for 1 day in the same solid to liquid ratio of 1:2000 (w/v), which is suggested as a method to release all Cr(VI) into the aqueous phase resulting from the dissolutions of the humus samples. The concentration of Cr(VI) in the NaOH solution was determined using the same method described above, but the blank control of distilled water was replaced by the supernatant to eliminate the colour influence of the dissolved humus samples.

2.3. Two-dimensional correlation spectroscopy analysis

To identify the functional groups species of different humus reacting with Cr(VI) and their reactivity (reaction sequence), the 2DCOS method (two-dimensional correlation spectroscopy) was used to analyse the FTIR spectra data of humus samples after reacting with Cr(VI) for different intervals. This spectroscopic analysis method was developed by Noda and Ozaki (Noda and Ozaki, 2005), and has been widely used in the fields of material science, food science and environmental science. The detailed analysis procedures and principles of this method have been stated in detail in our previous papers (Zhang et al., 2017; Zhang et al., 2018a; Zhang et al., 2018c). The 2DCOS analysis was produced using 2Dshige software (Kwansei-Gakuin University, Japan).

2.4. Kinetic model fitting

The pseudo-first-order kinetic model was utilized for the data analysis of Cr(VI) reduction by different humus fractions. The raw pseudo-first-order kinetic equation is shown as follows:

$$C_t = C_0 \cdot e^{-kt} \tag{1}$$

where C_t represents the variation of Cr(VI) concentration in the reaction system with time, including Cr(VI) in solution and Cr(VI) adsorbed on humus, C_0 represents the Cr(VI) initial concentration in the solution, and k represents the first-order reduction rate constant.

The amount of reduced Cr(III) is calculated by the difference between the initial and remaining Cr(VI) in the reaction system, which is shown as follows:

$$q_{re} = (C_0 - C_t)\eta \tag{2}$$

where q_{re} represents the amount of reduced Cr(III), C_0 represents the initial Cr(VI) concentration in the solution, C_t represents the variation of the Cr(VI) concentration in the reaction system, and η represents the solution volume to humus mass ratio (v:w).

The linear form of Eq. (2) is shown as follows:

$$\ln\left(1 - \frac{q_{re}}{\eta C_0}\right) = -kt \tag{3}$$

The slope of $\ln(1 - \frac{q_{re}}{\eta C_0})$ to $-t$ represents the reduction rate constant.

3. Results and discussion

3.1. Characteristics of different humus fractions

The particle size distributions of different humus fractions are shown in Fig. S1, and it was found that the particle size decreased with the progressive fractionation, namely HA > HMi > HMc > HMr, which can be further verified by the SEM images of the humus particles (Fig. S2). Additionally, the zero point of charge (pH_{pzc}) of different humus fractions is shown in Fig. S3. As indicated, the pH_{pzc} of HA, HMi and HMc ranged from 0.63 to 0.95, which implied that under pH 1 condition of this study, the surface of these humus particles were negatively charged. While the pH_{pzc} of HMr was determined to be 2.49, and this indicated that under the pH condition of this study the surface of HMr particles was positively charged.

With progressive humus fractionation, the bulk polarity of different fractions gradually decreased from 0.44 for HA to 0.35 for HMr (Table 1). This suggests that the fraction with a higher content of polar carbon was readily extracted in the humus fractionation process, which indicates that the apolar humus molecules were preferentially adsorbed onto minerals, which is consistent with the findings of the previous study (Wang and Xing, 2005). The $S_{(O+N)/C}/B_{(O+N)/C}$ ratio decreased with the progressive fractionation as well, which implied that the decrease in their surface polarity was much more evident than the bulk particles in this extraction process. However, it should be noted that the $S_{(O+N)/C}/B_{(O+N)/C}$ ratio for HMr increased significantly, which suggested the distinct properties of HMr compared with other humus fractions.

The contents of the bulk acidic groups, including carboxyl and phenol, decreased from 3.45 and 3.15 mmol g^{-1} for HA to 1.98 and 1.55 mmol g^{-1} for HMr, respectively, with progressive extractions, which is coordinated with the regularity of the bulk polarity. The composition of surface functionalities was determined according to XPS C1s spectra (Fig. S4). The proportion of O—C═O decreased with progressive fractionation; however, the C—O proportion of HMr increased significantly resulting in the increasing surface polarity. Considering the low phenolic groups content of HMr, it may be mainly enriched in polysaccharide (cellulose) structures containing relatively high contents of hydroxyl and ether.

To verify the potential distinct molecular structures of the HMr fraction, solid-state ^{13}C CP/MAS NMR was employed, and the results are shown in Fig. 1. It should be pointed out that the decoupling process for the NMR signals will increase the signal intensities of different types of carbons by various extents; therefore, the spectra can only be employed for semi-quantitative analysis and relative comparison among a series of related spectra. The NMR spectra of HA, HMi and HMc have similar shapes, which are all similar to the spectra published for soil HA samples (Bonin and Simpson, 2007), and only the peak intensities associated with alkoxy C (50–109 ppm) and carboxylic C (163–190 ppm) decreased slightly with progressive extractions (Table 1), which indicates that these fractions have similar molecular structural characteristics. However, the shape of the HMr spectrum is quite different from the other fractions, especially in the region of alkoxy C. The strong peaks at 73 and 105 ppm can be respectively attributed to ring carbons and anomeric carbon in cellulose (Ionescu et al., 2015; VanderHart and Atalla, 1984), which indicates that HMr has a higher content of cellulose structures. However, comparatively, the HA, HMi and HMc fractions have higher contents of primary alcohol/methoxyl (50–60 ppm) and secondary alcohol (65–80 ppm) structures. This further confirms that HMr is structurally different from the other humus fractions.

Additionally, the characteristic doublet peaks of amorphous (29–30 ppm) and crystalline (32–33 ppm) polymethylene chain carbons are significant in all fractions as shown in Fig. 1 (Chen et al., 2017). The crystalline polymethylene carbon was reported to be resistant to environmental attack, while the amorphous version is important in sorption processes (Hu et al., 2000). With progressive fractionation, it

Table 1
Bulk elemental composition and atomic ratios, bulk content of acidic groups, surface functional groups and elemental composition, and integrated solid-state ^{13}C CP/MAS NMR data of different humus fraction.

Samples	Elemental composition (%)				$B_{(O+N)/C}$[a]	Ash content (%)	–COOH (mmol g^{-1})[b]	–OH (mmol g^{-1})[b]
	C	H	O	N				
HA	56.41	3.91	28.51	4.14	0.44	1.49	3.45 (0.05)	3.15 (0.07)
HMi	57.83	4.89	27.14	4.54	0.42	1.26	3.55 (0.02)	2.55 (0.37)
HMc	58.99	4.31	26.91	3.41	0.39	1.14	3.77 (0.03)	1.97 (0.05)
HMr	47.24	3.44	19.94	1.57	0.35	22.86	1.98 (0.04)	1.55 (0.11)

Samples	Surface functional groups and elemental composition (%)[c]							$S_{(O+N)/C}$[d]
	C–C and C–H	C–O	C=O	O–C=O	C	N	O	
HA	41.77	12.56	6.27	9.67	70.27 (1.71)	4.62 (0.08)	25.12 (1.63)	0.45
HMi	46.59	10.15	7.76	7.73	72.24 (1.85)	5.61 (0.83)	22.15 (1.02)	0.38
HMc	53.53	9.93	6.94	7.53	77.93 (0.91)	2.75 (0.01)	19.32 (0.93)	0.28
HMr	43.64	12.87	8.55	5.80	70.86 (1.07)	3.83 (0.59)	25.32 (0.49)	0.41

Samples	Distribution of C chemical shift/ppm (%)[e]					Aromatic C[f] (%)	Polar C[f] (%)	Aromatic polar C[f] (%)
	0–50	50–109	109–145	145–163	163–190			
HA	25.49	17.43	32.11	4.51	20.46	57.08	42.40	24.97
HMi	37.16	15.30	25.75	3.76	18.04	47.54	37.09	21.79
HMc	33.03	10.23	43.12	3.23	10.38	56.73	23.84	13.61
HMr	28.83	24.94	37.27	2.76	6.19	46.22	33.89	8.95

[a] $B_{(O+N)/C}$: bulk polarity.
[b] Carboxylic and phenolic group contents determined by the titration method described elsewhere (Li et al., 2008).
[c] Determined by XPS analysis and the overlapping peaks resolving method.
[d] $S_{(O+N)/C}$: surface polarity.
[e] Determined by ^{13}C CP/MAS NMR analysis.
[f] Aromatic C: total aromatic region (109–163 ppm); Polar C: total polar carbon region (50–109 ppm and 145–190 ppm); Aromatic polar C: polar carbon in the aromatic region (145–190 ppm). The values in the brackets are the standard deviations of three independent measurements.

can be seen that the proportion of amorphous polymethylene carbon decreased, accompanied by the increase in crystalline polymethylene carbon, and this may be responsible for the relatively inert nature of humus associated with minerals compared with the dissociated one in soils and sediments.

3.2. Cr(VI) sorption to different humus fractions

To determine the adsorption processes of Cr(VI) onto different humus fractions, a kinetic batch experiment was conducted, and the results are shown in Fig. 2. It can be seen from Fig. 2(a) that the removal rate of Cr(VI) in solution decreased with progressive humus fractionation, namely, HA > HMi > HMc > HMr, and the maximum Cr (VI) removal quantities ranged from 2.42 to 3.86 mmol g^{-1} (125.84 to 200.72 mg g^{-1}) after 64 days. In theory, the decrease in Cr(VI) concentration in solution can be attributed to (i) its adsorption onto humus particles and (ii) its reduction into Cr(III) in the reaction system. Therefore, the quantity relationship among the different existing states of Cr (VI) and Cr(III) can be expressed as the following equation:

$$\Delta Cr(VI)_{aq} = Cr(VI)_{aq}{}^{0} - Cr(VI)_{aq} = Cr(VI)_{ad} + Cr(III)_{re} \quad (4)$$

where, $\Delta Cr(VI)_{aq}$ represents the decreasing quantity of Cr(VI) in solution; $Cr(VI)_{aq}^{0}$ represents the initial Cr(VI) quantity in solution;

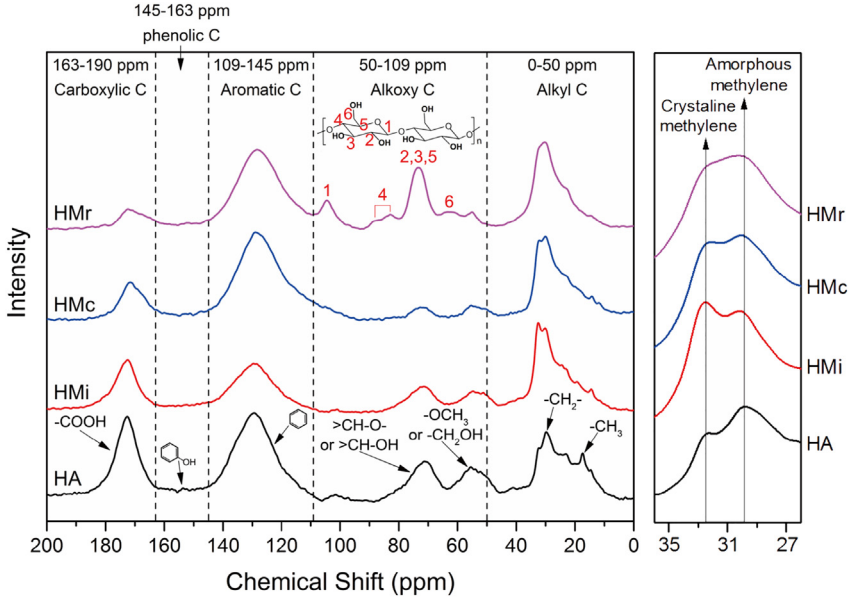

Fig. 1. Solid-state ^{13}C CP/MAS NMR spectra of different humus fractions.

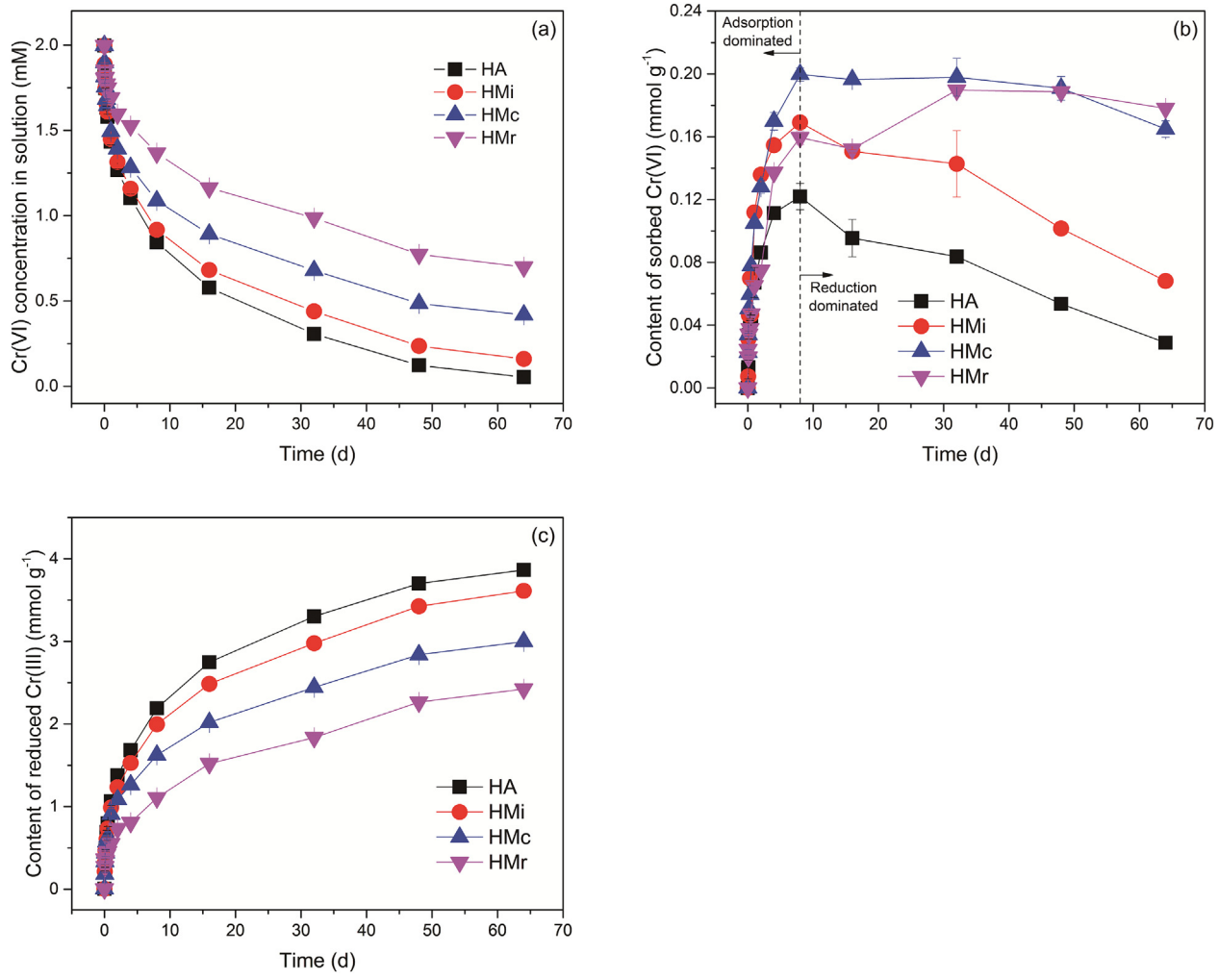

Fig. 2. (a) Concentration variation of Cr(VI) in solutions induced by different humus fractions, (b) content variation of sorbed Cr(VI) on different humus fractions, and (c) content variation of reduced Cr(III) in the reaction system induced by different humus fractions.

$Cr(VI)_{aq}$ represents the Cr(VI) quantity variaition with time in solution; $Cr(VI)_{ad}$ represents the adsorbed Cr(VI) quantity on humus particles; and $Cr(III)_{re}$ represents the reduced Cr(III) quantity in the reaction system.

As the value of $Cr(VI)_{aq}^{0}$ is a constant and the $Cr(VI)_{aq}$ can be determined directly in the solution, the determinations of $Cr(VI)_{ad}$ and $Cr(III)_{re}$ are required. Considerting that the $Cr(III)_{re}$ may exist both on humus particles and in solution, the determination of $Cr(VI)_{ad}$ is considered to be a much more direct way to illustrate the adsorption and reduction processes of Cr(VI) by different humus fractions, because once the $Cr(VI)_{ad}$ was obtained, the $Cr(VI)_{re}$ can be determined according to Eq. (4) as well.

To determine the sorbed Cr(VI) content on humus particles, the humus samples, after reacting with Cr(VI), were fully dissolved in 0.1 M NaOH to release the Cr(VI) anions into the aqueous phase for the Cr(VI) concentration determination (HMr cannot be dissolved in alkaline solutions, but it has been suggested that nearly all Cr(VI) anions can be desorbed back to aqueous phase under extremely alkaline solutions due to the high exchange ability of OH^- for Cr(VI) anions), and the results are shown in Fig. 2(b). As indicated, a certain amount of Cr still existed in the sorbed Cr(VI) form on humus particles, which is consistent with the findings of our previous study (Zhang et al., 2018a). The contents of sorbed Cr(VI) for different humus fractions all obviously increased over 8 days. After 8 days, the sorbed Cr(VI) contents of HA, HMi and HMc decreased to various degrees, but it was almost unchanged for HMr. The maximum Cr(VI) adsorption quantities of different humus fractions ranged from 0.12 to 0.20 mmol g^{-1} (6.24 to 10.4 mg g^{-1}), accounting for approximately 3%–5% of the total Cr in the reaction system, which means that the majority of sorbed Cr(VI) was reduced into Cr(III). This can be further supported by the XPS Cr2p spectra of humus samples after reacting with Cr(VI) (Fig. S5). The reduced Cr(III) in the system can be determined by the difference between the initial and remaining content of Cr(VI) in the system, and the results are shown in Fig. 2(c). It can be seen that the reduction rate significangly decreased with progressive humus fractionation, and follows the order HA > HMi > HMc > HMr.

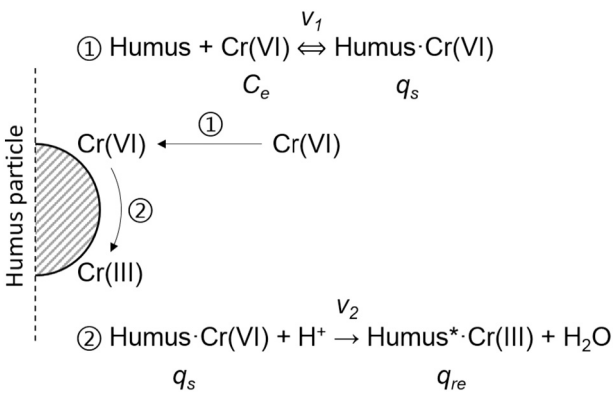

Fig. 3. Scheme of Cr(VI) adsorption and reduction by undissolved humus.

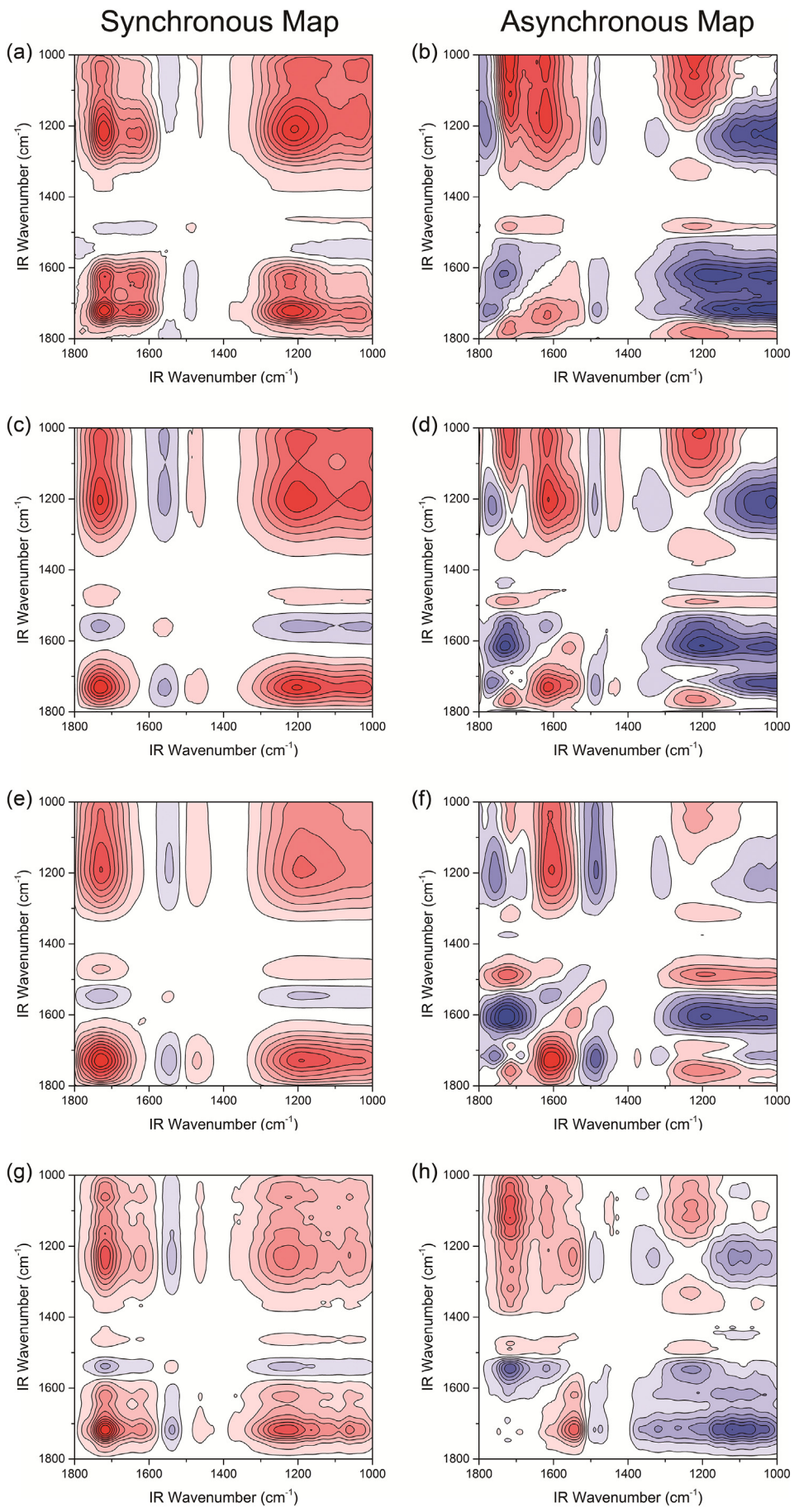
Synchronous Map
Asynchronous Map
(a)
(b)
(c)
(d)
(e)
(f)
(g)
(h)
IR Wavenumber (cm-1)
1000
1200
1400
1600
1800

According to the pH_{pzc} of different humus fractions (as shown in Fig. S3), under the pH condition of this study, the surfaces of HA, HMi and HMc were all negatively charged, therefore, the Cr(VI) anion (mainly $HCrO_4^-$, as shown in Fig. S6) more tended to be adsorbed onto the surfaces of these fractions by chemical bonding force (ligand exchange) instead of electrostatic attraction force. While the surface of HMr was positively charged, and then the electrostatic adsorption and chemical adsorption might work together in Cr(VI) adsorption processes.

The retention of Cr(VI) by humus has been determined to follow an adsorption-reduction mechanism in our previous studies (Barnie et al., 2018; Zhang et al., 2017), and the scheme is shown in Fig. 3. (i) The Cr (VI) in the aqueous phase is adsorbed onto the humus particle surface, forming ion exchangeable and binding Cr(VI); (ii) the sorbed Cr(VI) is reduced into Cr(III) by adjacent reductive functional groups; and (iii) the reduced Cr(III) is complexed by functionalities on the humus or released into the aqueous phase. The reduction of Cr(VI) by humus in solution can be neglected, because the TOC (total organic carbon) concentration of the dissolved humus, acting as electron donor for Cr (VI) reduction in solution, only account for approximately 3% of the total mass under the same pH condition (Zhang et al., 2018a), which will be much lower for the undissolved HMr. Consequently, the sorbed Cr(VI) can be considered as a required medium for Cr(VI) reduction by humus. The adsorption rate (v_1) is mainly determined by the difference between the Cr(VI) concentration in the aqueous phase (C_e) and the corresponding theoretical content of sorbed Cr(VI) in the solid phase (q_s), and the linear balanced relationship between C_e and q_s is determined by the partition coefficient K_d. While the reduction rate (v_2) is jointly determined by the sorbed Cr(VI) concentration (q_s), the content of reductive functional groups and the protons, and in this experimental condition (constant pH, as shown in Fig. S8) the reduction rate is mainly related to q_s for each humus fraction.

As shown in Fig. 2(b), at the initial stage, the difference between C_e and q_s is relatively high, resulting in an adsorption rate (v_1) that was higher than the reduction rate (v_2), and thus, the content of sorbed Cr (VI) accumulated within 8 days, which can be called the "adsorption-dominated" period. After 8 days, the Cr(VI) concentration in the solution decreased significantly, making the adsorption rate (v_1) smaller than the reduction rate (v_2), and thus, the content of sorbed Cr(VI) decreased gradually, which can be called the "reduction-dominated" period. Considering that the content of sorbed Cr(VI) is limited by the maximum adsorption capacity of each humus fraction, the reduction of sorbed Cr(VI) plays a crucial role in the removal of Cr(VI) from the aqueous phase by humus, because the quantity of reduction (2.42–3.86 mmol g^{-1}) is far higher than that of Cr(VI) adsorption (0.12–0.20 mmol g^{-1}). The reduction quantities of different humus fractions are considered to be directly related to the composition of their functional groups, and therefore, the determination of functionality species for Cr(VI) reduction by different humus fractions is of crucial importance for clarifying the underlying mechanisms.

3.3. The role of functional group types for Cr(VI) reduction by different humus fractions

To identify the functional group variations of different humus fractions while reacting with Cr(VI), FTIR was utilized to characterize the changes in functional groups with time, and the results are shown in Fig. S7. As indicated, at the initial time, different humus fractions have similar spectral shapes, and the absorbance peaks at 1709, 1465, 1379, 1228 and 1031 cm^{-1} are significant, which are attributed to carboxyl, methylene, methyl, phenol and hydroxyl, respectively (Fanning and Vannice, 1993; Li et al., 2003; O'Reilly and Mosher, 1983; Sellitti et al., 1990). The spectral shape of HMr is a little different from that of the other fractions, especially at bands of 1379 cm^{-1}, and the sharp peak indicates that HMr has a much higher methyl content, which is consistent with its aliphatic and hydrophobic nature. The peaks at 1709 and 1228 cm^{-1} decreased significantly with time for all fractions, and the peak at 1545 cm^{-1}, which is assigned to the carboxyl complexed by Cr, obviously increased (Zhao et al., 2016). However, the intensity changes in the peaks at 1465, 1348 and 1031 cm^{-1} are not evident, and thus, 2DCOS analysis was emplolyed to identify these subtle changes.

Table 2
The peak assignment and sign relationship between synchronous and asynchronous maps of different humus fractions.

Position (cm^{-1})	Peak assignment	Sign[a]				
		1709	1545	1465	1379	1228
1709	Carboxyl					
1545	Chelated carboxyl	++++				
1465	Methylene	++++	++++			
1379	Methyl	++++	++++	----		
1228	Phenol	++++	----	----	----	
1031	Hydroxyl	++++	----	----	----	++++

[a] Signs were obtained in the upper-left corner of the maps: +, same sign; −, opposite sign. The order of signs is associated with progressive fractionation, namely, HA, HMi, HMc and HMr.

As shown in Fig. 4, the synchronous and asynchronous maps for different fractions are almost similar in the peak distributions. Five major auto peaks can be identified at 1709, 1545, 1228 and 1031 cm^{-1} along the diagonal line of the synchronous maps as shown in Fig. 4(a, c, e, g), and the cross peaks at 1465 and 1379 cm^{-1} in the upper-left corner of the synchronous and asynchronous maps can be identified as well. Additionally, a majority of the cross peaks of the synchronous maps had a positive sign, except for the cross peak associated with 1545 cm^{-1}. This indicated that mainly carboxyl (1707 cm^{-1}), phenol (1228 cm^{-1}), hydroxyl (1031 cm^{-1}) methyl (1379 cm^{-1}) and methylene (1465 cm^{-1}) participated in the reaction with Cr(VI), and the reduced Cr(III) might be complexed by carboxyl producing chelated carboxyl (1545 cm^{-1}).

To verify the absorbance changing orders of related peaks, the sign relationship between synchronous and asynchronous maps and peak assignments are summarized in Table 2. It can be seen that all humus fractions have the same signs for two different corresponding bands, which indicates that the functional groups for different humus fractions have the same preferential orders participating in the reaction with Cr (VI) according to the rules defined by Noda (Noda and Ozaki, 2005), namely, carboxyl (1709 cm^{-1}) > phenol (1228 cm^{-1}) > hydroxyl (1031 cm^{-1}) > chelated carboxyl (1545 cm^{-1}) > methyl (1379 cm^{-1}) > methylene (1465 cm^{-1}). As indicated, the functional groups of different humus fractions follow a similar mechanism for Cr(VI) adsorption and reduction. The orders of phenol, hydroxyl, methyl and methylene are coordinated with their chemical reducibility, which indicates that these functional groups may sequentially act as the main electron donors in different reaction stages. Additionally, it should be noted that the reducibility of carboxyl is far weaker than phenol and hydroxyl. However, why has carboxyl participated in the reaction prior to other functional groups? In other words, was carboxyl truly oxidized in the reaction? According to our previous study (Zhang et al., 2018a), carboxyl was considered to more likely act as a ligand for Cr complexation instead of being oxidized, which was supported by the XPS C1s spectra. Hence, it is of great value to verify this conclusion from other perspectives.

Fig. 4. 2DCOS analysis of FTIR spectra of different humus fractions after reacting with Cr(VI). (a), (c), (e) and (g) are respectively the synchronous maps of HA, HMi, HMc and HMr. (b), (d), (f) and (h) are respectively the asynchronous maps of HA, HMi, HMc and HMr.

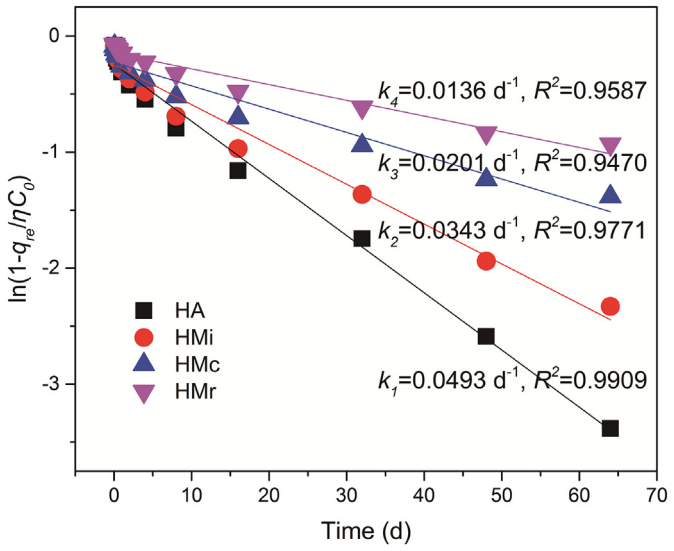

Fig. 5. Fitting of the reduction rate constant *k* for Cr(VI) reduction by different humus fractions with a pseudo-first-order kinetic model.

3.4. Correlation between the reduction rate constants and humus properties

The reduction of Cr(VI) by different humus fractions was described by pseudo-first-order kinetics, and the linear relationship ($R^2 > 0.94$) between the logarithmic concentration of Cr(VI) and the reaction time is shown in Fig. 5. As indicated, the reduction rate constant *k* decreased from 0.0493 to 0.0136 d^{-1} with progressive humus fractionation. It should be pointed out that this fitting approach did not take into consideration the adsorption process of Cr(VI) by humus, however, an overall reaction rate parameter independent of the Cr(VI) concentration can be obtained, which is only related to the molecular structures of humus. This method will be favoured, revealing the relationship between the overall reduction rate and the microscaled domain arrangement of humus.

To gain insight into the relationship between the reduction rate constant *k* and humus acidic groups, surface functionalities, polarity and aromaticity, a linear correlation analysis was applied to the corresponding data, and the results are shown in Fig. 6. It can be seen from Fig. 6 (a) that the *k* values for different humus fractions are positively correlated with the contents of phenolic groups as shown by the solid blue line ($R^2 = 0.99$), but negatively correlated with carboxylic groups as shown by the dashed black line ($R^2 = 0.95$, except for HMr), which further confirms that phenol, instead of carboxyl, is the most important electron donor for Cr(VI) reduction by all humus fractions. Although a strong correlation between *k* and the phenol content is found, it should be noted that the regression line does not go through the origin, which indicates that a nonlinear relationship may exist within the low phenol content range from 0 to 1.5 mmol g^{-1}.

As shown in Fig. 6(b), *k* values for different humus fractions are positively correlated with the surface carboxylic groups proportion as shown by the solid blue line (O—C═O, $R^2 = 0.89$), but negatively correlated with the surface apolar carbon proportion as shown by the

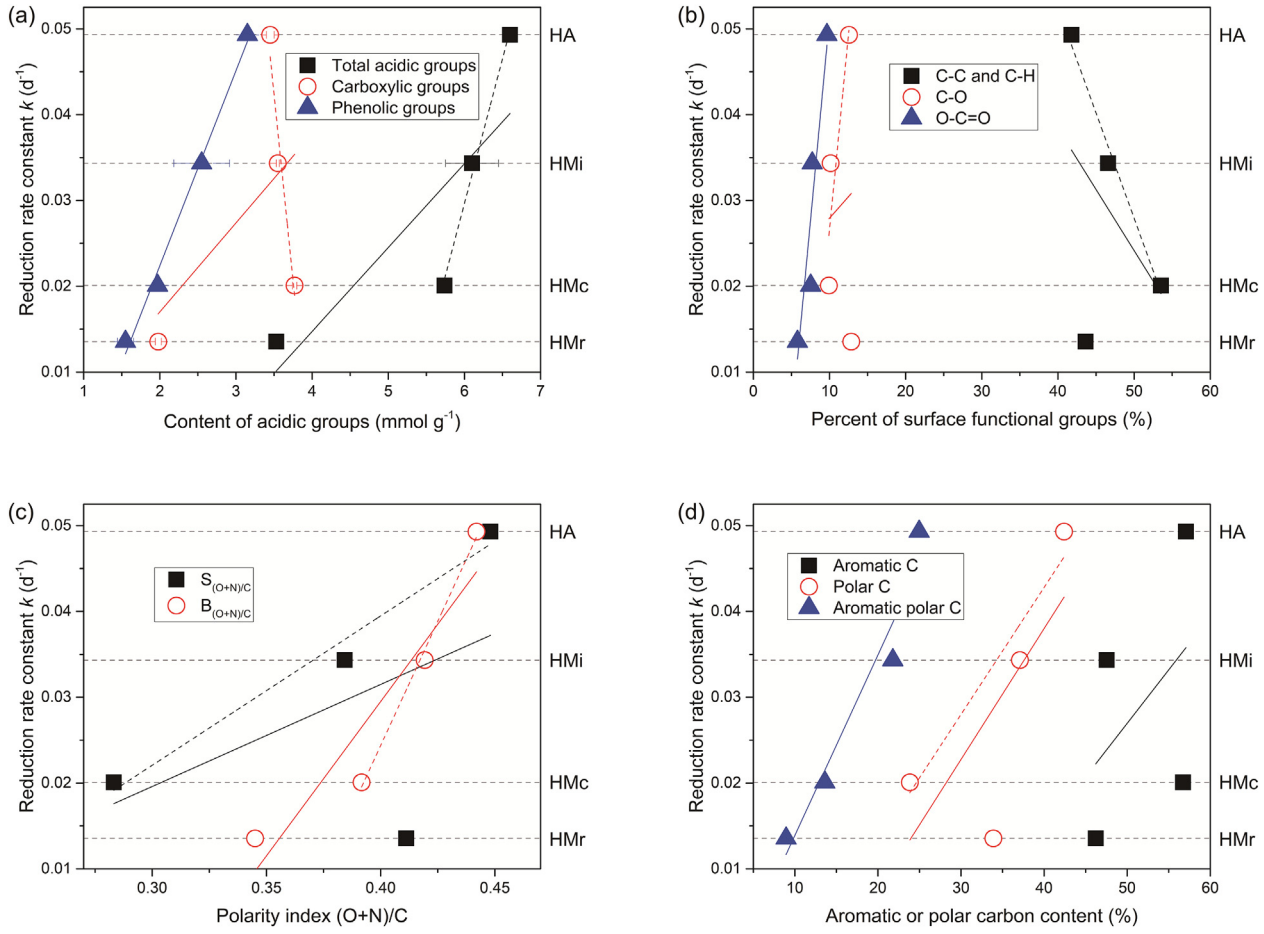

Fig. 6. Correlation relationship between the reduction rate constant *k* of Cr(VI) by different humus fractions and (a) the content of acidic groups, (b) the percentage of surgace functional groups, (c) the polarity index (O + N)/C, and (d) the aromatic or polar carbon content. The solid line represents the correlation among all humus fractions, and the dashed line represents the correlation among HA, HMi, and HMc (except for HMr).

dashed black line (C—C and C—H, $R^2 = 0.99$, except for HMr). The content of the surface carboxylic groups may be associated with the affinity of humus for Cr(VI) complexation, because carboxyl has been reported to participate in the complexation of Cr(VI) (Brose and James, 2013), which is considered as a precondition for Cr(VI) reduction by organic matter (Elovitz and Fish, 1995). On the other hand, the higher proportion of apolar carbon means a lower proportion of oxygen-containing polar carbon, which is crucial for Cr(VI) reduction, and the nonlinear characteristics of HMr (a lower proportion of surface apolar carbon resulting in a lower reduction rate) further implies its distinct properties from other fractions.

Except for HMr, the *k* values for the HA, HMi and HMc fractions are both positively correlated with their surface and bulk polarity as shown by the dashed lines in Fig. 6(c) ($R^2 = 0.98$ and 0.99, respectively), and this implies that both surface and bulk polarity can be employed for the estimation of the Cr(VI) reduction capabilities by HA-type humus, which coincides with the correlation of total acidic groups as shown in Fig. 6(a). The overall results of surface polarity are complementary with that of the surface apolar carbon proportion shown in Fig. 6(b), and the surface polarity of HMr is much higher than that predicted by the linear rule developed from HA-type humus. This coincides with the results above that the HMr surface has a higher content of cellulose structures (enriched in polar carbon but lacking in polar oxygen-containing functionalities), which has been proven to be quite resistant to Cr(VI) attack in our previous study (Zhang et al., 2018b).

The *k* values of different humus fractions have a poor correlation relationship with the proportions of aromatic carbon ($R^2 = 0.21$), and this indicates that the aromaticity and aliphaticity of humus are not directly related to their reducibility for Cr(VI). Additionally, *k* values have a strong correlation with the proportions of aromatic polar carbon ($R^2 = 0.95$); however, a weak correlation between the *k* values and the proportions of total polar carbon ($R^2 = 0.56$) is obtained due to the nonlinear characteristics of HMr. This finding indicated that the Cr(VI) reduction is more dependent on the aromatic polar functionalities, and the resistance of the cellulose structures of HMr can account for its nonlinear nature.

4. Conclusions

HA, HMi and HMc are the same type of humus with similar molecular structures, and only the content of polar oxygen-containing functional groups decreased with progressive humus fractionation. HMr is structurally distinct from the other fractions with a high content of cellulose, probably resulting from the humification of plant cell walls, which tend to be resistant to Cr(VI) oxidation. Hence, in soil environment HA-type humus has a higher ability to reduce Cr(VI) when compared with HMr fraction, and the reduction rate of Cr(VI) is mainly determined by the content of phenolic groups instead of carboxylic groups. Except for HMr, the Cr(VI) reduction rates of different humus fractions were also positively correlated with the surface and bulk polarity, but not with aromaticity or aliphaticity. Additionally, the humin fractions linked to iron oxides and clay (HMi and HMc) were investigated in this study in their monomer form; however, the associations of humus with minerals might change their interface characteristics, resulting in a further influence on the retention effect of Cr(VI) migration in soils and sediments, which is of great value for further study.

Conflicts of interest

There are no competing interests to declare.

Acknowledgements

This work was financially supported by the National Natural Science Foundation of China (41672239), National Key R&D Program of China (2017YFF0205804), National Science and Technology Major Project (2016ZX05040-002-003), and China Geological Survey (1212011121173). We also would like to thank Lingli Wang, Lihui Wu, Dongjie Gu from Sinomine Rock and Mineral Analysis (Tianjin) Co., Ltd. for their help on the extraction of humus.

Appendix A. Supplementary data

Supplementary data to this article can be found online at https://doi.org/10.1016/j.scitotenv.2018.10.165.

References

Barnie, S., Zhang, J., Wang, H., Yin, H., Chen, H., 2018. The influence of pH, co-existing ions, ionic strength, and temperature on the adsorption and reduction of hexavalent chromium by undissolved humic acid. Chemosphere 212, 209–218.
Bonin, J.L., Simpson, M.J., 2007. Variation in phenanthrene sorption coefficients with soil organic matter fractionation: the result of structure or conformation? Environ. Sci. Technol. 41, 153–159.
Brose, D.A., James, B.R., 2013. Hexavalent chromium reduction by tartaric acid and isopropyl alcohol in Mid-Atlantic soils and the role of Mn(III,IV) (hydr)oxides. Environ. Sci. Technol. 47, 12985–12991.
Chen, S.Y., Huang, S.W., Chiang, P.N., Liu, J.C., Kuan, W.H., Huang, J.H., et al., 2011. Influence of chemical compositions and molecular weights of humic acids on Cr(VI) photoreduction. J. Hazard. Mater. 197, 337–344.
Chen, W., Wang, H., Gao, Q., Chen, Y., Li, S., Yang, Y., et al., 2017. Association of 16 priority polycyclic aromatic hydrocarbons with humic acid and humin fractions in a peat soil and implications for their long-term retention. Environ. Pollut. 230, 882–890.
Dai, J., Becquer, T., Rouiller, J.H., Reversat, G., Bernhard-Reversat, F., Lavelle, P., 2004. Influence of heavy metals on C and N mineralisation and microbial biomass in Zn-, Pb-, Cu-, and Cd-contaminated soils. Appl. Soil Ecol. 25, 99–109.
Dermentzis, K., Christoforidis, A., Valsamidou, E., Lazaridou, A., Kokkinos, N., 2011. Removal of hexavalent chromium from electroplating wastewater by electrocoagulation with iron electrodes. Glob. NEST J. 13, 412–418.
Dhal, B., Thatoi, H.N., Das, N.N., Pandey, B.D., 2013. Chemical and microbial remediation of hexavalent chromium from contaminated soil and mining/metallurgical solid waste: a review. J. Hazard. Mater. 250-251, 272–291.
Dou, S., Xiao, Y., Zhang, J., 2006. Quantities and structural characteristics of various fractions of soil humin. Acta Pedol. Sin. 43, 934–940.
Elovitz, M.S., Fish, W., 1995. Redox interactions of Cr(VI) and substituted phenols: products and mechanism. Environ. Sci. Technol. 29, 1933–1943.
Fabbri, D., Chiavari, G., Galletti, G.C., 1996. Characterization of soil humin by pyrolysis(/methylation) gas chromatography mass spectrometry: structural relationships with humic acids. J. Anal. Appl. Pyrolysis 37, 161–172.
Fanning, P.E., Vannice, M.A., 1993. A drifts study of the formation of surface groups on carbon by oxidation. Carbon 31, 721–730.
Guo, X., Wang, X., Zhou, X., Ding, X., Fu, B., Tao, S., et al., 2013. Impact of the simulated diagenesis on sorption of naphthalene and 1-naphthol by soil organic matter and its precursors. Environ. Sci. Technol. 47, 12148–12155.
Hayes, M.H.B., Mylotte, R., Swift, R.S., 2017. Chapter two — Humin: its composition and importance in soil organic matter. In: Sparks, D.L. (Ed.), Advances in Agronomy. 143. Academic Press, pp. 47–138.
Hori, M., Shozugawa, K., Matsuo, M., 2015. Reduction process of Cr(VI) by Fe(II) and humic acid analyzed using high time resolution XAFS analysis. J. Hazard. Mater. 285, 140–147.
Hsu, C.-L., Wang, S.-L., Tzou, Y.-M., 2007. Photocatalytic reduction of Cr(VI) in the presence of NO_3^- and Cl^- electrolytes as influenced by Fe(III). Environ. Sci. Technol. 41, 7907–7914.
Hsu, N.H., Wang, S.L., Lin, Y.C., Sheng, G.D., Lee, J.F., 2009. Reduction of Cr(VI) by crop-residue-derived black carbon. Environ. Sci. Technol. 43, 8801–8806.
Hsu, L.C., Wang, S.L., Lin, Y.C., Wang, M.K., Chiang, P.N., Liu, J.C., et al., 2010. Cr(VI) removal on fungal biomass of *Neurospora crassa*: the importance of dissolved organic carbons derived from the biomass to Cr(VI) reduction. Environ. Sci. Technol. 44, 6202–6208.
Hu, W.-G., Mao, J., Xing, B., Schmidt-Rohr, K., 2000. Poly(methylene) crystallites in humic substances detected by nuclear magnetic resonance. Environ. Sci. Technol. 34, 530–534.
Huang, S.W., Chiang, P.N., Liu, J.C., Hung, J.T., Kuan, W.H., Tzou, Y.M., et al., 2012. Chromate reduction on humic acid derived from a peat soil—exploration of the activated sites on HAs for chromate removal. Chemosphere 87, 587–594.
Ionescu, A., Hurduc, M., Stroia, V., Oprişor, M., Heine, G., 2015. Solid-state NMR investigations of cellulose structure and interactions with matrix polysaccharides in plant primary cell walls. J. Exp. Bot. 20, 333–338.
Janos, P., Hula, V., Bradnova, P., Pilarova, V., Sedlbauer, J., 2009. Reduction and immobilization of hexavalent chromium with coal- and humate-based sorbents. Chemosphere 75, 732–738.
Jardine, P.M., Fendorf, S.E., Mayes, M.A., Larsen, I.L., Brooks, S.C., Bailey, W.B., 1999. Fate and transport of hexavalent chromium in undisturbed heterogeneous soil. Environ. Sci. Technol. 33, 2939–2944.
Kang, S., Xing, B., 2008. Humic acid fractionation upon sequential adsorption onto goethite. Langmuir 24, 2525–2531.
Tsutsuki, Kiyoshi, Kuwatsuka, Shozo, 2012. Characterization of humin-metal complexes in a buried volcanic ash soil profile and a peat soil. Soil Sci. Plant Nutr. 38, 297–306.

Li, L., Huang, W.L., Peng, P., Sheng, G.Y., Fu, J.M., 2003. Chemical and molecular heterogeneity of humic acids repetitively extracted from a peat. Soil Sci. Soc. Am. J. 67, 740–746.
Li, Y., Yue, Q., Gao, B., Li, Q., Li, C., 2008. Adsorption thermodynamic and kinetic studies of dissolved chromium onto humic acids. Colloids Surf. B: Biointerfaces 65, 25–29.
Li, C.L., Gao, S.Q., Gao, Q., Wang, L.C., Zhang, J.J., 2015. Characterization of bulk soil humin and its alkaline-soluble and alkaline-insoluble fractions. Rev. Bras. Ciênc. Solo 39, 120–126.
Lin, Y.C., Wang, S.L., Shen, W.C., Huang, P.M., Chiang, P.N., Liu, J.C., et al., 2009. Photoenhancement of Cr(VI) reduction by fungal biomass of *Neurospora crassa*. Appl. Catal. B Environ. 92, 294–300.
Liu, J., Zhang, X.H., Tran, H., Wang, D.Q., Zhu, Y.N., 2011. Heavy metal contamination and risk assessment in water, paddy soil, and rice around an electroplating plant. Environ. Sci. Pollut. Res. 18, 1623–1632.
Noda, I., Ozaki, Y., 2005. Two-dimensional Correlation Spectroscopy: Applications in Vibrational and Optical Spectroscopy. John Wiley & Sons.
O'Reilly, J.M., Mosher, R.A., 1983. Functional groups in carbon black by FTIR spectroscopy. Carbon 21, 47–51.
Pallo, F., 1993. Evolution of organic matter in some soils under shifting cultivation practices in Burkina Faso. In: Mulongoy, K., Merckx, R. (Eds.), Soil Organic Matter Dynamics and the Sustainability of Tropical Agriculture. John Wiley and Sons, pp. 109–120.
Rice, J.A., 2001. Humin. Soil Sci. 166, 848–857.
Rice, J., Maccarthy, P., 1989. Isolation of humin by liquid-liquid partitioning. Sci. Total Environ. 81–82, 61–69.
Sellitti, C., Koenig, J.L., Ishida, H., 1990. Surface characterization of graphitized carbon-fibers by attenuated total reflection Fourier-transform infrared-spectroscopy. Carbon 28, 221–228.
Song, J.Z., Peng, P., Huang, W.L., 2005. Characterization of humic acid-like material isolated from the humin fraction of a topsoil. Soil Sci. 170, 599–611.
Song, G., Hayes, M.H., Novotny, E.H., Simpson, A.J., 2011. Isolation and fractionation of soil humin using alkaline urea and dimethylsulphoxide plus sulphuric acid. Naturwissenschaften 98, 7–13.
Specht, C.H., Kumke, M.U., Frimmel, F.H., 2000. Characterization of NOM adsorption to clay minerals by size exclusion chromatography. Water Res. 34, 4063–4069.
Tavares Rosa, L.M., Botero, W.G., Caldas Santos, J.C., Cacuro, T.A., Waldman, W.R., do Carmo, J.B., et al., 2018. Natural organic matter residue as a low cost adsorbent for aluminum. J. Environ. Manag. 215, 91–99.
Van Zomeren, A., Comans, R.N., 2007. Measurement of humic and fulvic acid concentrations and dissolution properties by a rapid batch procedure. Environ. Sci. Technol. 41, 6755–6761.
VanderHart, D.L., Atalla, R.H., 1984. Studies of microstructure in native celluloses using solid-state ^{13}C NMR. Macromolecules 17, 1465–1472.
Wang, K., Xing, B., 2005. Structural and sorption characteristics of adsorbed humic acid on clay minerals. J. Environ. Qual. 34, 342–349.
Wang, X., Guo, X., Yang, Y., Tao, S., Xing, B., 2011. Sorption mechanisms of phenanthrene, lindane, and atrazine with various humic acid fractions from a single soil sample. Environ. Sci. Technol. 45, 2124–2130.
Wang, Y., Li, L., Zou, X., Shu, R., Ding, L., Yao, K., et al., 2016. Impact of humin on soil adsorption and remediation of Cd(II), Pb(II), and Cu(II). Soil Sediment Contam. 25, 700–715.
Wen, B., Zhang, J.J., Zhang, S.Z., Shan, X.Q., Khan, S.U., Xing, B., 2007. Phenanthrene sorption to soil humic acid and different humin fractions. Environ. Sci. Technol. 41, 3165–3171.
Wittbrodt, P.R., Palmer, C.D., 1995. Reduction of Cr(VI) in the presence of excess soil fulvic acid. Environ. Sci. Technol. 29, 255–263.
Wittbrodt, P.R., Palmer, C.D., 1996. Effect of temperature, ionic strength, background electrolytes, and Fe(III) on the reduction of hexavalent chromium by soil humic substances. Environ. Sci. Technol. 30, 2470–2477.
Wittbrodt, P.R., Palmer, C.D., 1997. Reduction of Cr(VI) by soil humic acids. Eur. J. Soil Sci. 48, 151–162.
Xiao, W., Zhang, Y., Li, T., Chen, B., Wang, H., He, Z., et al., 2012. Reduction kinetics of hexavalent chromium in soils and its correlation with soil properties. J. Environ. Qual. 41, 1452–1458.
Xing, B.S., Liu, J.D., Liu, X.B., Han, X.Z., 2005. Extraction and characterization of humic acids and humin fractions from a black soil of China. Pedosphere 15, 1–8.
Yan, M., Ma, J., Ji, G., 2016. Examination of effects of Cu(II) and Cr(III) on Al(III) binding by dissolved organic matter using absorbance spectroscopy. Water Res. 93, 84–90.
Yang, Y., Shu, L., Wang, X., Xing, B., Tao, S., 2011. Impact of de-ashing humic acid and humin on organic matter structural properties and sorption mechanisms of phenanthrene. Environ. Sci. Technol. 45, 3996–4002.
Zeng, F., Ali, S., Zhang, H., Ouyang, Y., Qiu, B., Wu, F., et al., 2011. The influence of pH and organic matter content in paddy soil on heavy metal availability and their uptake by rice plants. Environ. Pollut. 159, 84–91.
Zhang, J., He, M., Shi, Y., 2009. Comparative sorption of benzo[alpha]phrene to different humic acids and humin in sediments. J. Hazard. Mater. 166, 802–809.
Zhang, J.J., Wang, S., Wang, Q.H., Wang, N., Li, C.L., Wang, L.C., 2013. First determination of Cu adsorption on soil humin. Environ. Chem. Lett. 11, 41–46.
Zhang, J., Chen, L., Yin, H., Jin, S., Liu, F., Chen, H., 2017. Mechanism study of humic acid functional groups for Cr(VI) retention: two-dimensional FTIR and ^{13}C CP/MAS NMR correlation spectroscopic analysis. Environ. Pollut. 225, 86–92.
Zhang, J., Yin, H., Chen, L., Liu, F., Chen, H., 2018a. The role of different functional groups in a novel adsorption-complexation-reduction multi-step kinetic model for hexavalent chromium retention by undissolved humic acid. Environ. Pollut. 237, 740–746.
Zhang, J., Yin, H., Wang, H., Xu, L., Samuel, B., Liu, F., et al., 2018b. Reduction mechanism of hexavalent chromium by functional groups of undissolved humic acid and humin fractions of typical black soil from Northeast China. Environ. Sci. Pollut. Res. 25, 16913–16921.
Zhang, J., Yin, H.L., Samuel, B., Liu, F., Chen, H.H., 2018c. A novel method of three-dimensional hetero-spectral correlation analysis for the fingerprint identification of humic acid functional groups for hexavalent chromium retention. RSC Adv. 8, 3522–3529.
Zhao, T.T., Ge, W.Z., Nie, Y.X., Wang, Y.X., Zeng, F.G., Qiao, Y., 2016. Highly efficient detoxification of Cr(VI) by brown coal and kerogen: process and structure studies. Fuel Process. Technol. 150, 71–77.
Zhou, T., Wu, L., Luo, Y., Christie, P., 2018. Effects of organic matter fraction and compositional changes on distribution of cadmium and zinc in long-term polluted paddy soils. Environ. Pollut. 232, 514–522.